Journal of the European Ceramic Society 22 (2002) 1177–1182

www.elsevier.com/locate/jeurceramsoc

Effect of In-doping on the microstructure and CH_4-sensing ability of porous $CaZrO_3$/MgO composites

Yoshikazu Suzuki*, Masanobu Awano, Naoki Kondo, Tatsuki Ohji

Synergy Materials Research Center, National Institute of Advanced Industrial Science and Technology (AIST), 2268-1, Shimo-shidami, Moriyama-ku, Nagoya 463-8687, Japan

Received 17 May 2001; accepted 10 July 2001

Abstract

Porous In-doped $CaZrO_3$/MgO composites (nominally, $CaZr_{0.95}In_{0.05}O_{2.975}$/MgO and $CaZr_{0.90}In_{0.10}O_{2.95}$/MgO) were prepared by pressureless reactive sintering of $CaMg(CO_3)_2$, ZrO_2 and In_2O_3 with 0.5 mass% LiF additive. The In-doped composites had a uniform open-porous microstructure, similarly to the porous $CaZrO_3$/MgO composites as reported before, but their pore-size became slightly larger. The CH_4-sensing properties both in argon and air atmospheres were investigated at 600–900 °C. It was found that the In-doping was effective to increase the CH_4-sensitibity in air for all temperature range, whereas it decreased the CH_4-sensitibity in argon. These results can be qualitatively explained by the increase in oxygen vacancies induced by the In-doping.

Keywords: $CaZrO_3$/MgO; MgO; Perovskites, Rietveld analysis; Sensors

1. Introduction

Calcium zirconate, $CaZrO_3$, is an attractive material for high-temperature structural applications because of its high-melting temperature (~2370 °C) and physical/chemical stability.[1–3] Besides its refractory nature, it has fascinating electrical properties originated from the perovskite-type crystal structure, and can be used for sensors and other electric devises. For example, In-doped $CaZrO_3$ can be applied to proton-conductive electrolytes,[4–7] humidity sensors[4,8] and hydrogen sensors,[4,9] while pure $CaZrO_3$ for high-temperature thermistors[10] and CH_4 sensors[11]. Chiang et al.[11] reported that pure $CaZrO_3$ showed dramatic response to methane (CH_4) with the sensitivity increasing with increasing temperature.

Recently, the present authors have developed uniformly open-porous $CaZrO_3$/MgO composites with three-dimensional (3-D) network structure, via pressureless reactive sintering of $CaMg(CO_3)_2$ and ZrO_2 with 0.5 mass% LiF additive.[12] The porous composites maintained the open-porous structure up to high temperatures (typically ~1400 °C), because of their unique 3-D structure and the good chemical compatibility between $CaZrO_3$ and MgO (eutectic temperature: ~2050 °C[13,14]). It has also been confirmed that the porous $CaZrO_3$/MgO composites show the rapid response to methane in an argon atmosphere.[15] Thus, owing to the good structural stability and the gas-sensitivity, the porous $CaZrO_3$/MgO composites are expected to be multi-functional filter materials, i.e. simultaneous hot gas-filtering and hot gas-sensing in one component. For the practical uses, however, sufficient CH_4 sensitivity in "air" is indispensable.

In this study, we report the effect of the In-doping on microstructure and CH_4-sensitivity of the porous $CaZrO_3$/MgO composites. The sensitivity both in argon and air atmospheres are evaluated and discussed.

2. Experimental procedure

2.1. Sample preparation

High-purity natural dolomite, $CaMg(CO_3)_2$ (<75 μm),[16,17] un-doped ZrO_2 (Sumitomo Cement Co. Ltd., 99.9%), In_2O_3 (Kojundo Chemical Laboratory Co.

* Corresponding author. Tel.: +81-52-739-0156; fax: +81-52-739-0136.

E-mail address: y-suzuki@aist.go.jp (Y. Suzuki).

0955-2219/02/$ - see front matter
PII: S0955-2219(01)00405-8

Ltd., 99.99%) and LiF (Wako Pure Chemical Ind. Ltd., 99.9%) powders were used as starting materials; $CaMg(CO_3)_2$, ZrO_2 and In_2O_3 were weighed to be the desired compositions of $CaZrO_3$/50 mol% MgO (hereinafter, In-0), $CaZr_{0.95}In_{0.05}O_{2.975}$/50 mol% MgO (In-5) and $CaZr_{0.90}In_{0.10}O_{2.95}$/50 mol% MgO (In-10). LiF (0.5 mass% to total starting powders) was added to form liquid phase during sintering to enhance the reactivity and neck-growth.[12] These powders were wet-ball milled in ethanol for 6 h by using a planetary ball-mill process (acceleration: 6 g). The mixed slurry was dried, subsequently dry-ball-milled for 24 h, and sieved through a 100-mesh screen. The mixed powder was cold isostatically pressed at 200 MPa after mold-pressing. The green compacts (15 mm in diameter and $\sim$ 5 mm in thickness) were sintered in air at 1300 °C for 2 h to obtain the porous composites. An Al_2O_3 container was used in order to enlarge CO_2 partial pressure during the decomposition of dolomite, which suppressed the excess shrinkage.[15]

2.2. Characterization

Constituent phases of the sintered composite were analyzed by an X-ray rotating anode diffractometer (Model Rotaflex, Rigaku), operated at 40 kV and 100 mA. The microstructure of the composites was characterized using a scanning electron microscope (SEM, Model 6330F, JEOL). The porosity and the pore-size distribution were determined by mercury porosimetry (Poresizer 9320, Micromeritics, Norcross, GA, USA). Mercury intrusion was carried out at pressures between 0 and 207 MPa. Cylindrical pore model[18] was used for the calculation of the total pore volume (V_p), specific surface area (S_p), median pore diameter ($D = 4\ V_p/S_p$), and porosity (P).

Platinum wires were attached on the surface of porous composites with Pt paste, and used as electrodes for two-probe electrical measurements, since Pt is stable with the $CaZrO_3$–MgO system up to high temperatures (at least up to 1100 °C[19]). Pt-wired samples were heat-treated in air at 950 °C for 1 h to satisfy the sufficient connectivity. The electrical measurement was conducted at 600–900 °C with a DC voltage of 1 V. The gas flow rate was 200 ml/min and controlled by a mass flow meter. A reference gas (argon or air) and a CH_4 gas (1000 ppm, balanced by the reference gas) were alternatively introduced to the chamber. Current between two electrodes was measured by a picoammeter, and the resistance value was calculated by using Ohm's law.

3. Results and discussion

3.1. Constituent phases

Fig. 1 shows the XRD patterns for the porous in situ composites sintered at 1300 °C: (a) In-0 (nominally, $CaZrO_3$/MgO), (b) In-5 ($CaZr_{0.95}In_{0.05}O_{2.975}$/MgO) and (c) In-10 ($CaZr_{0.90}In_{0.10}O_{2.95}$/MgO). The XRD analysis revealed that the composites In-0 and In-5 were composed of only $CaZrO_3$ and MgO phases. However, for the composite In-10, the existence of $CaIn_2O_4$ phase was also confirmed (see the week peek at $2\theta \sim 33°$). The $CaIn_2O_4$ content in the composite In-10 was estimated to be $\sim$ 3 mass%, by using the Rietveld method (see the following section). Le and Rij et al.[20,21] recently reported that the heat-treatment at a relatively high temperature (1550 °C, 10 h) was needed to obtain single-phase $CaZr_{0.9}In_{0.1}O_{3-\alpha}$ even by the wet-chemical processing.

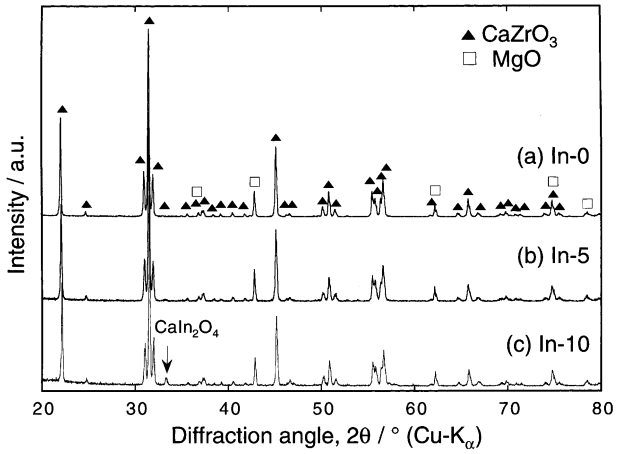

Fig. 1. XRD patterns of the porous in situ composites sintered at 1300 °C: (a) In-0 (nominally, $CaZrO_3$/MgO), (b) In-5 (nominally, $CaZr_{0.95}In_{0.05}O_{2.975}$/MgO) and (c) In-10 (nominally, $CaZr_{0.90}$ $In_{0.10}$ $O_{2.95}$/MgO).

3.2. Quantitative XRD analysis

The diffraction profiles were refined by the Rietveld method using *RIETAN-97* code programmed by Izumi.[22,23] Mass fraction of phases was determined by Rietveld method[24] as well, and it was converted into the molar fraction. Reported crystallographic parameters of $CaZrO_3$[25] and MgO[26] were utilized as the initial parameters of the refinement. For the composite In-10, the calculation was conducted by taking into account the $CaIn_2O_4$ phase. According to the report by Reid,[27], $CaIn_2O_4$ has the $CaFe_2O_4$-type crystal structure (orthorhombic, Pnma) and it is isomorphous with $CaSc_2O_4$.[28,29] Thus, fractional atomic coordinates of $CaSc_2O_4$[29] were employed for the calculation of $CaIn_2O_4$. As an example, Fig. 2 shows the observed and calculated XRD patterns for the composite In-10 (nominally $CaZr_{0.90}In_{0.10}O_{2.95}$/MgO) sintered at 1300 °C. Goodness-of-fit indicator,[30] S, was 1.1–1.3 for all composites, which suggests the analysis was sufficiently accurate for such purposes as the determinations of lattice-parameters and phase compositions.

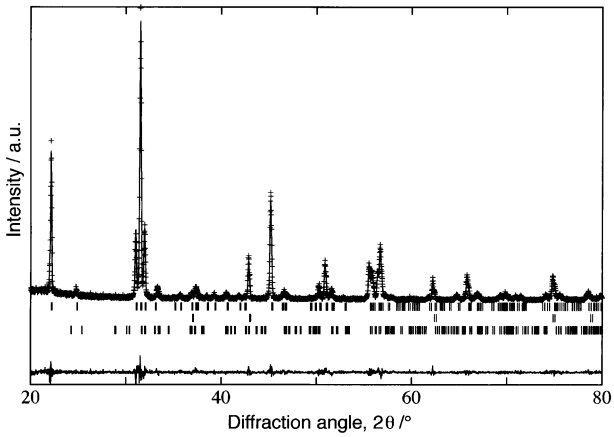

Fig. 2. Observed (+) and calculated (solid line) profile intensities of the composite In-10 sintered at 1300 °C. Differences between the two intensities are plotted at the bottom of the diagram. Short vertical bars below the pattern represent Bragg reflection positions for $CaZrO_3$ phase (top row), MgO phase (middle row) and $CaIn_2O_4$ phase (bottom row).

Table 1
Refined lattice parameters of $CaZrO_3$ and MgO phases in the porous composites sintered at 1300 °C

	Refs. 25,26	In-0	In-5	In-10
$CaZrO_3$ phase, Pnma				
a (Å)	5.7616 (2)	5.758 (5)	5.75 (1)	5.743 (1)
b (Å)	8.0171 (1)	8.017 (7)	8.01 (1)	8.000 (1)
c (Å)	5.5912 (1)	5.593 (5)	5.59 (1)	5.580 (1)
MgO phase, Fm3m				
a (Å)	4.213	4.215 (3)	4.215 (7)	4.206 (1)

Lattice parameters of $CaZrO_3$ and MgO phases determined by the Rietveld refinement are listed in Table 1. The change in the lattice parameters of $CaZrO_3$ with In-doping was relatively small ($\leqslant 0.2\%$), which can be explained by (1) the small difference in the ionic radii of Zr^{4+} and In^{3+} (supposing 6-fold coordination, Ahrens' ionic radii are 0.79 and 0.81 Å, respectively[31]) and (2) the formation of oxygen vacancies. The MgO lattice parameter in In-10 increased $\sim 2\%$, which suggests some In^{3+} dissolved in MgO. Note that the Ahrens' ionic radius of Mg^{2+} at 6-fold coordination is 0.66 Å.[31]

The compositions calculated from the Rietveld analysis are listed in Table 2. For the composites In-0 and In-5, the molar fraction was $CaZrO_3$:MgO = 50.0:50.0, which demonstrates that following reaction completely proceeded.

$$CaMg(CO_3)_2 + (1-x)ZrO_2 + xInO_{1.5} \rightarrow CaZr_{1-x}In_xO_{3-0.5x} + MgO + 2\ CO_2 \quad (1)$$

For In-10, it is somewhat difficult to determine the accurate composition because of the coexistence of $CaIn_2O_4$ phase and the MgO-$InO_{1.5}$ solid solubility. The phasic composition was estimated to be $CaZrO_3$(ss):MgO (ss):$CaIn_2O_4 \sim 77 \pm 2{:}20 \pm 2{:}3$ (in mass%), corresponding to $\sim 46 \pm 2{:}53 \pm 2{:}1$ (in mol%).

Table 2
Calculated phasic composition of the porous composites

Composition	In-0 $CaZrO_3$: MgO	In-5 $CaZrO_3$ (ss)[a]: MgO	In-10 $CaZrO_3$(ss)[a]: MgO (ss):$CaIn_2O_4$
In mass%	81.6:18.4	81.7:18.3	$77 \pm 2{:}20 \pm 2{:}3$
In mol%	50.0:50.0	50.0:50.0	$\sim 46 \pm 2{:}53 \pm 2{:}1$

[a] Nominal chemical compositions of $CaZr_{0.95}In_{0.05}O_{2.975}$ and $CaZr_{0.90}In_{0.10}O_{2.95}$ were used for the refinement and the determination of the phasic composition.

3.3. Microstructure

Fig. 3 shows SEM micrographs of the porous composites: (a) In-5 (porosity:60%) and (b) In-10 (porosity 57%). Microstructure of the porous $CaZrO_3$/MgO composites without In-doping was described in detail in our previous works.[12,15] The microstructure of In-5 and In-10 basically resembles to each other, but In-10 appears to be more homogeneous on the whole. Although they seem to have a sort of "3-D network structure," the network became coarser compared with the composites without In-doping (very narrow pore-size distribution, and pore-size of ~ 1.0 μm).[12,15] These phenomena are attributable to the increase in the liquid-phase content during the in situ processing by the In_2O_3 addition, which enhances the localized shrinkage, and thus, yield larger pores.

Fig. 4 demonstrates the pore-size distribution measured by mercury porosimetry. The pore-size distribution agreed well with the above SEM observation.

3.4. CH_4-sensing property

CH_4-sensing properties of the three composites (In-0, In-5 and In-10) both in argon and air background gases were evaluated. The sensitivities (R_0/R) of various conditions are plotted in Fig. 5. For example, the top curve in Fig. 5 (In-0 in Ar) was determined from the original response curves in Fig. 6 as is described below.

3.4.1. In-0 in Ar

Fig. 6 shows the response curves of the composite In-0 (porosity 50%) to 1000 ppm CH_4 balanced by Ar at 600–800 °C. The resistance of the porous composite decreased on exposure to CH_4 gas, as is reported by Chiang et al.,[11] and returned back to the almost original level by removing the CH_4 gas. A possible sensing mechanism is deduced as follows. It is reported that undoped $CaZrO_3$ is a p-type semiconductor (significantly at high oxygen partial pressure), and when doped with

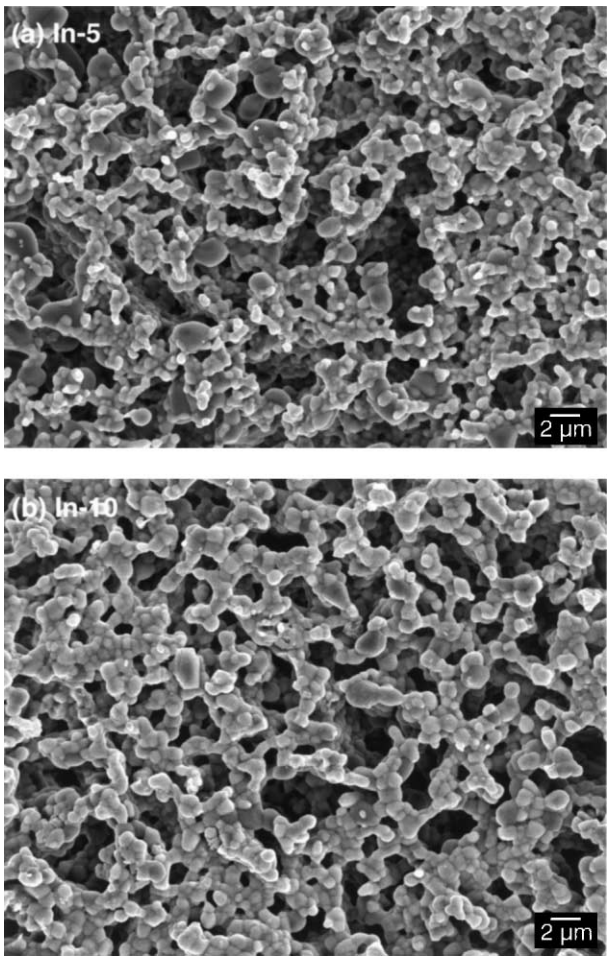

Fig. 3. Scanning electron micrographs of the porous composites: (a) In-5 and (b) In-10. Microstructure of porous $CaZrO_3$/MgO composite without In-doping was described in previous works.[12,15]

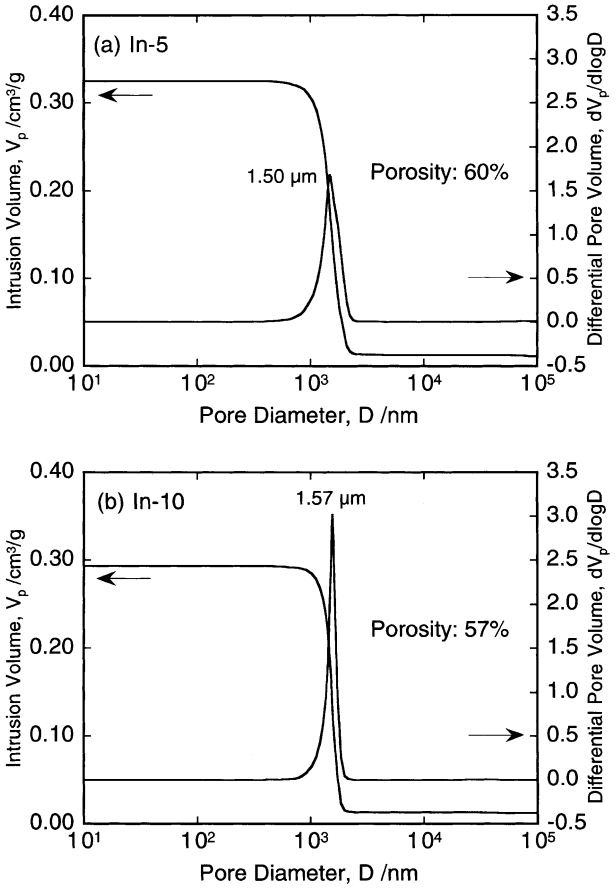

Fig. 4. Pore-size distribution determined by mercury porosimetry for the porous composites: (a) In-5 and (b) In-10.

oxides such as Al_2O_3, Y_2O_3 and MgO or with a small excess of CaO or ZrO_2, it becomes a hole-oxygen ion mixed conductor (predominantly with oxygen-ion conduction).[10,32] In this study, when the background gas is argon, $CaZrO_3$ in the porous composite is thought to be an oxide-ion conductor since MgO coexisted with $CaZrO_3$. In this case, the reductive atmosphere increases the oxygen vacancy near the surface, which can explain the decrease in resistance upon the exposure to reductive CH_4 gas as observed in Fig. 6.

3.4.2. In-0 in air

When the measurement was conducted in air, the sensitivity remarkably decreased ($R_0/R \sim 1.1$ at 700–900 °C) as shown in the bottom curve in Fig. 5. In addition, at 600 °C, the resistance of In-0 increased on the exposure to CH_4 gas ($R/R_0 = 1.04$, and thus, $R_0/R = 0.96$). These results suggest that the contribution of ionic conductivity decreases and that of hole (i.e. p-type conduction) increases in air, particularly at a low temperature.

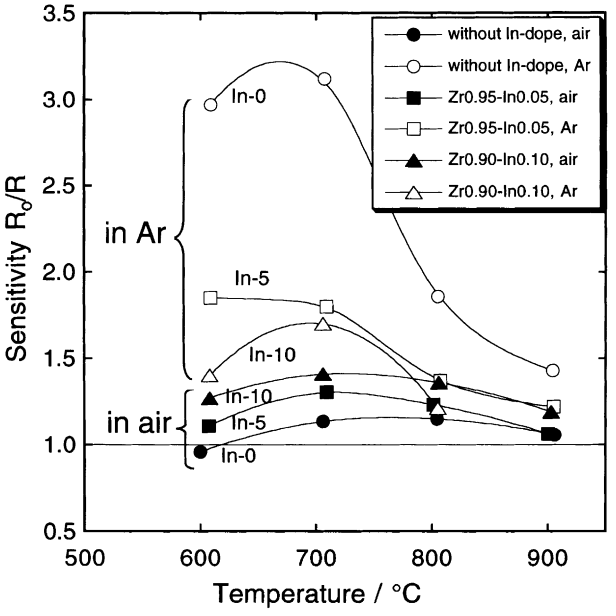

Fig. 5. Variation of sensitivity (R_0/R) with temperature for In-0, In-5 and In-10 in argon and air atmospheres; R_0: resistance in a reference gas, R: resistance in 1000-ppm CH_4.

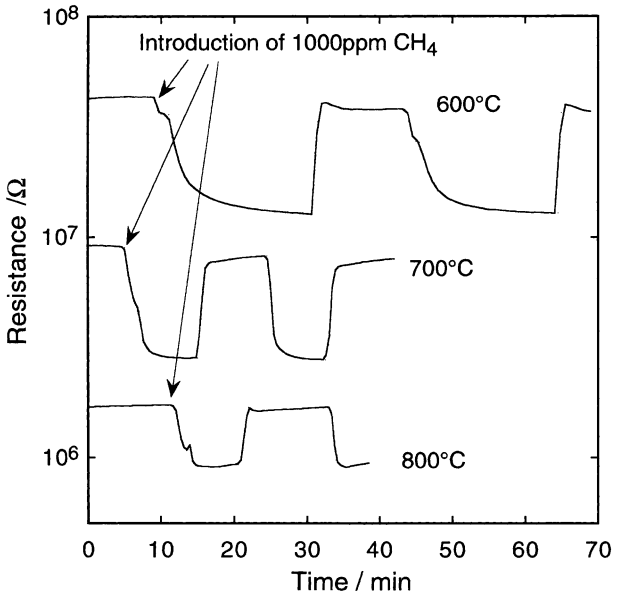

Fig. 6. Response curves of the porous $CaZrO_3$/MgO composite (In-0, porosity: 50%) to 1000 ppm CH_4 (balanced by Ar) at 600–800 °C.

3.4.3. In-5 and In-10 in Ar

In the argon atmosphere, the CH_4-sensitivity decreased with increasing indium content. This result can be explained by a following mechanism. With In-doping, since the content of oxygen vacancies increased, the absolute resistance value decreased via the increase in carrier density, and the contribution of ionic conductivity increased. Due to the *absolute* increase in oxygen vacancies, the effect of reductive gas (1000 ppm CH_4) became *relatively* smaller.

3.4.4. In-5 and In-10 in air

In contrast, in the air atmosphere, the CH_4-sensitivity increased with increasing indium content. In air, it can be assumed that the oxygen adsorption prevents the CH_4 adsorption. However, by the increase in the oxygen vacancies via In-doping, the number of active adsorption sites may increase. This may be a reason of increase in the CH_4-sensitivity in air by the In-doping.

4. Conclusions

The effect of In-doping on microstructure and CH_4-sensing property of porous $CaZrO_3$/MgO composites was studied. In conclusion:

1. The composites In-0 (nominally, $CaZrO_3$/MgO) and In-5 ($CaZr_{0.95}In_{0.05}O_{2.975}$/MgO) consisted of only $CaZrO_3$ and MgO phases. On the other hand, the composite In-10 (nominally, $CaZr_{0.90}In_{0.10}O_{2.95}$/MgO) was composed of $CaZrO_3$, MgO and $CaIn_2O_4$ ($\sim$ 3 mass%).
2. The effect of In-doping on lattice constants of $CaZrO_3$ was rather small due to the similar ionic radii of Zr^{4+} and In^{3+}.
3. By the In-doping, the pore-size became a little larger presumably caused by the progress of localized liquid phase sintering.
4. Although the In-doping decreased the CH_4-sensitivity in argon, it was effective to improve the CH_4-sensitivity in air.

Acknowledgements

This work was supported by METI, Japan, as part of the Synergy Ceramics Project. The authors are members of the Joint Research Consortium of Synergy Ceramics.

References

1. De Pretis, A., Ricciardiello, F. and Sbaizero, O., *Mater. Sci. Eng.*, 1985, **71**, 166.
2. De Pretis, A., Ricciardiello, F. and Sbaizero, O., *Powder Metall. Int.*, 1986, **18**, 427–430.
3. Hou, T. I. and Kriven, W. M., *J. Am. Ceram. Soc.*, 1994, **77**, 65–72.
4. Yajima, T., Iwahara, H., Koide, K. and Yamamoto, K., *Sens. Actuators*, 1991, **B5**, 145–147.
5. Kurita, N., Fukatsu, N., Ito, K. and Ohashi, T., *J. Electrochem. Soc.*, 1995, **142**, 1552–1559.
6. Kobayashi, K., Yamaguchi, S. and Iguchi, Y., *Solid State Ionics*, 1998, **108**, 355–362.
7. Yamaguchi, S., Kobayashi, K., Higuchi, T., Shin, S. and Iguchi, Y., *Solid State Ionics*, 2000, **136-137**, 305–311.
8. Engelen, W., Buekenhoudt, A., Luyten, J. and De Schutter, F., *Solid State Ionics*, 1997, **96**, 55–59.
9. Yajima, T., Koide, K., Takai, H., Fukatsu, N. and Iwahara, H., *Solid State Ionics*, 1995, **79**, 333–337.
10. Wang, C. C., Akbar, S. A., Chen, W. and Schorr, J. R., *Sens. Actuators*, 1997, **A58**, 237–243.
11. Chiang, Y., Wang, C. C. and Akbar, S. A., *Sens. Actuators*, 1998, **B46**, 208–212.
12. Suzuki, Y., Morgan, P. E. D. and Ohji, T., *J. Am. Ceram. Soc.*, 2000, **83**, 2091–2093.
13. De Aza, S., Richmond, C. and White, J., *Trans. J. Br. Ceram. Soc.*, 1974, **73**, 109–116.
14. Yin, Y. and Argent, B. B., *J. Phase Equilibria*, 1993, **14**, 588–600.
15. Suzuki, Y., Awano, M., Kondo, N. and Ohji, T., *J. Ceram. Soc. Jpn.*, 2001, **109**, 79–81.
16. Suzuki, Y., Morgan, P. E. D., Sekino, T. and Niihara, K., *J. Am. Ceram. Soc.*, 1997, **80**, 2949–2953.
17. Suzuki, Y., Morgan, P. E. D. and Niihara, K., *Powder Diffraction*, 1998, **13**, 216–221.
18. Ishizaki, K., Komarneni, S. and Nanko, M., *Porous Materials—Process Technology and applications*. Kluwer Academic Press, Dordrecht, 1998.
19. Suzuki, Y., Morgan, P. E. D. and Ohji, T., *Ceram. Eng. Sci. Proc.*, in press.
20. Le, J., van Rij, L. N., van Landschoot, R. C. and Schoonman, J., *J. Eur. Ceram. Soc.*, 1999, **19**, 2589–2591.
21. van Rij, L., Winnubst, L., Jun, L. and Schoonman, J., *J. Mater. Chem.*, 2000, **10**, 2515–2521.

22. Kim, Y.-I. and Izumi, F., *J. Ceram. Soc. Jpn.*, 1994, **102**, 401–404.
23. Xiao, Y., Hayakawa, S., Gohshi, Y., Oshima, M., Izumi, F., Okudera, H., Toraya, H. and Ohsumi, K., *Powder Diffraction*, 1999, **14**, 106–110.
24. Hill, R. J. and Howard, C. J., *J. Appl. Crystallogr*, 1987, **20**, 467–474.
25. Koopmans, H. J. A., Van de Velde, G. M. H. and Gellings, P. J., *Acta Crystallogr*, 1983, **C39**, 1323–1325.
26. Sasaki, S., Takeuchi, Y. and Fujino, K., *Proc. Jpn. Acad.*, 1979, **55**, 43–48.
27. Reid, A. F., *Inorg. Chem.*, 1967, **6**, 631–633.
28. Müller-Buschbaum, H. and Schnering, H. G., *Z. Anorg. Allgem. Chem.*, 1965, **336**, 295–305.
29. Horyn, R. and Lukaszewicz, K., *Bull. Acad. Pol. Sci-Chim.*, 1966, **14**, 499–504.
30. Young, R. A. (ed.), In *The Rietveld Method.* Oxford University Press, Oxford, 1993, pp. 1–38.
31. Ahrens, L. H., *Geochim. Cosmochim. Acta*, 1952, **2**, 155.
32. De Pretis, A., Longo, V., Ricciardiello, F. and Sbaizero, O., *Silicates Industriels*, 1984, **7-8**, 139.